Engineering Science & Technology
http://ojs.wiserpub.com/index.php/EST/

UNIVERSAL WISER PUBLISHER

Research Article

MHD Non-Aligned Stagnation-Point Flow of Nanofluid over a Stretching Surface with a Convective Boundary Condition

Asha S. Kotnurkar*, Gayitri Mali

Department of Mathematics, Karnatak University, Dharwad-58000, Karnataka, India
Email: as.kotnur2008@gmail.com

Received: 24 September 2022; **Revised:** 3 November 2022; **Accepted:** 23 November 2022

Abstract: In the present paper, MHD non-aligned stagnation-point flow is found to be interesting and innovative in the analysis of viscous nanofluids over a stretching surface with a convective boundary condition in presence of the porous medium. Due to its many engineering and industrial uses, such as cooling nuclear reactors during an emergency shutdown, soft sheet extrusion, metal spinning, and solar central receivers exposed to wind current, the study of oblique stagnation point flow is important. A suitable similarity transformation is utilized for the reduction of a set of governing equations, which are solved using the Differential Transformation Method (DTM) with Maple software. The Nusselt number (Nu_x), skin friction (C_f), and Sherwood number (Sh_x) are tabulated. A strong agreement is seen, and the accuracy of the results tabulated using DTM and the numerical method (fourth-order Runge-Kutta-Fehlberg integration scheme) is illustrated. Further, velocity, temperature, and nanoparticle volume fraction profiles are shown graphically and studied under various parameters. It is reported that the magnetic parameter reduces the axial and oblique velocity gradients while enhancing the temperature and volume fraction profiles. The porosity parameter reduces the axial and oblique velocity gradients while enhancing the temperature profile.

***Keywords*:** non-aligned stagnation-point flow, stretching surface, porous medium, magnetic effect, DTM

Nomenclature

$\hat{\hat{u}}$, $\hat{\hat{v}}$ Velocity components in the x- and y- axis, respectively ($m \cdot s^{-1}$)
x, y Cartesian coordinates measured along the stretching sheet (m)
$\hat{\hat{C}}_W$ Nanoparticle concentration at the stretching surface ($mol \cdot m^{-3}$)
D_b Brownian diffusion coefficient
$\hat{\hat{C}}_\infty$ Nanoparticle concentration far from the sheet ($mol \cdot m^{-3}$)
D_T Thermophoresis diffusion coefficient
f Dimensionless stream function
h_f Convective heat transfer coefficient ($W \cdot m^{-2} \cdot K^{-1}$)
$\hat{\hat{C}}$ Nanoparticle concentration ($mol \cdot m^{-3}$)

DOI: https://doi.org/10.37256/est.4120231965

$\hat{\hat{T}}_\infty$ Temperature of the fluid far away from the stretching sheet (K)
k Thermal conductivity of the nanofluids ($W \cdot m^{-1} \cdot K^{-1}$)
g Oblique stream function component
Re_x Local Reynolds number
$\hat{\hat{T}}$ Fluid temperature (K)
q_w Surface heat flux ($W \cdot m^{-2}$)
K Permeability coefficient of the porous medium (m^2)
q_m Surface mass flux ($kg \cdot s^{-1} \cdot m^{-2}$)
$\hat{\hat{T}}_f$ Temperature of the hot fluid (K)
B_0 Magnetic field strength (T)

Greek symbols

α_f Thermal diffusivity ($m^2 \cdot s^{-1}$)
ψ Stream function ($m^2 \cdot s^{-1}$)
μ_f Dynamic viscosity of the base fluid ($kg \cdot m^{-1} \cdot s^{-1}$)
v_f Kinematic viscosity ($m^2 \cdot s^{-1}$)
ρ_f Density of the fluid ($kg \cdot m^{-3}$)
τ The ratio of the nanoparticle heat capacity and the base fluid heat capacity
p Pressure ($N \cdot m^{-2}$)
ϕ Dimensionless nanoparticle volume fraction
β Volumetric coefficient of thermal expansion
ρ_p Density of the nanoparticle ($kg \cdot m^{-3}$)
β^* Volumetric concentration coefficient

1. Introduction

In several industrial and engineering processes, the prominent importance of flow and heat transfer over stretching sheets can be seen. For instance, in polymer sheets extrusion, production of glass-fiber and paper, wire drawing, metal-spinning, etc. Because the final product's quality depends on how quickly heat is transported from the fluid to the stretching surface during cooling or heating. As a result, selecting an appropriate cooling or heating liquid is crucial because it directly affects the rate of heat transfer. The theory of flow over a stretching plate was coined by Crane [1]. While in certain circumstances a solid wall will stop the flow, in others a free stagnation point or line will be found inside the fluid domain. The entire horizontal axis of a stagnation point is covered by a solid or stretched wall in stagnation point flow, and the fluid's domain is $y > 0$. This simple model of an oblique stagnation point assists us to know how a boundary layer forms. As a result, the position of the stagnation point is essential for understanding boundary layer behavior. Due to its many engineering and industrial applications, such as cooling nuclear reactors during an emergency shutdown, soft sheet extrusion, metal spinning, and solar central receivers exposed to wind current, the study of this oblique stagnation point flow has attracted researchers' interest [2]. Stuart [3] originally investigated the flow approaching a fixed rigid surface at its oblique stagnation point. Later, Tamada [4] and Dorrepaal [5] independently examined this problem. Reza and Gupta [6] expanded Chiam's [7] work on sheets with oblique stagnation point flow. Recently some considerable investigations on oblique stagnation-point flows can be seen in [8]-[13].

A solid matrix with a continuous network of pores is referred to as a porous medium. Natural materials such as sand, wood, human lungs, etc. are examples of porous media that permit fluid flow. Flowing through a porous media became the focus of some researches over the past few decades due to its multiple physical and industrial uses. In material processing, fuel cell equipment, and geothermal energy, among other applications, the flow over a porous medium is especially important. Interest in this subject has been greatly sparked by the fact that thermally driven flows in porous media have several applications in chemical and mechanical engineering, including food processing and

storage, geophysical systems, underground disposal of nuclear, etc. Raptis and Takhar [14] were among the first to investigate the flow through a porous medium. Seddeek [15] investigated the heat and mass transfer on a sheet through the porous medium. Rehman et al. [16] studied the flow of nanofluids over an exponential sheet. Some other interesting papers on a porous medium in various geometries and effects can be seen in [17]-[21].

The analysis of the MHD flow of an electrically conducting fluid due to a stretching surface is essential in current metallurgy and metal-working processes. Such types of flows also occur in industrial equipment like MHD generators, pumps, gas turbines, power generators, the regulation of boundary layers in aerodynamics, crystal formation, etc. Examples of these fields include the cooling of the first wall within a nuclear reactor containment vessel, where the magnetic field is used to shield the hot plasma from the wall, and the magnetic field-assisted metal fusion process in an electrical furnace [22]. Mahapatra and Gupta [23] and Ishak [24] both looked at MHD stagnation point flow in the direction of a surface. Furthermore, Rajendar et al. [25] studied MHD flow due to nanofluid over an exponential sheet. Some other works regarding the magnetic effect can be seen in [26]-[29].

Nanofluid is said to be a composite of a solid-liquid mixture of nanoparticles of sizes 1-100 nm. It consists of a liquid called base fluid such as ethyl glycol, water, oil, etc., and solid particles known as nanoparticles. Nanofluids can significantly improve the base fluid's capacity for heat transfer. Because heat transfer is an essential step in both physics and engineering, improvements in its properties will raise the performance of a variety of operations. As a result, nanofluids have numerous industrial uses, including as lubricants, coolants, heat exchangers, and micro-channel heat sinks. According to these applications, the term "nanofluids" was first investigated by Choi [30]. The use of nanofluids is essential due to their high thermal conductivity properties. Some studies on nanofluids can be seen in [31]-[35].

The Differential Transform Approach (DTM), a powerful semi-exact method, is used in the current paper. Zhou [36], who addressed linear and non-linear issues in electrical circuit issues, was the first to propose this approach. DTM has expanded over the years. This technique was created in 1999 by Chen and Ho [37] for PDE's with two independent variables. The two-dimensional DTM was expanded into the three-dimensional DTM by Ayaz [38] in 2004. In 2005, Arikoglu and Ozkol [39] used the DTM for integrodifferential equations. Fractional differential equations and Telegraph equations have both been solved using this method. This method for solving nonlinear ODEs has been employed by many writers recently [40]-[42]. DTM is therefore superior to other techniques in several ways. DTM is unaffected by small or large quantities. As a result, DTM can be directly used to solve nonlinear problems with governing equations and boundary/initial conditions. In the Homotopy Analysis Method (HAM), we compute auxiliary parameters by using h-curves but DTM does not need them. HAM needs initial guesses and an auxiliary linear operator to solve equations but DTM solves equations directly.

From the above-mentioned literature, the problem of MHD non-aligned stagnation point flow of nanofluids over a stretching surface is discussed. But, how the porous medium influences the MHD non-aligned stagnation point flow towards a stretching sheet in nanofluids with convective boundary conditions using DTM is not yet studied. This work aims to close the perceived research gaps in nanofluids. The numerical method (fourth-order Runge-Kutta-Fehlberg integration scheme with shooting technique) and DTM are used to tabulate the findings. A good agreement is obtained. Here, equations are solved using DTM.

2. Mathematical formulation

A steady, incompressible, two-dimensional flow of a nanofluid through a porous medium in a boundary layer over a convectively heated stretched sheet at $y = 0$ is shown in Figure 1. Two equal and opposing forces stretch the sheet across the x-axis while keeping the origin stationary with velocity $\hat{\hat{U}}_W(x) = cx$. Let $\hat{\hat{U}}_\infty(x) = ax + by$ be the fluid's speed beyond the boundary layer. B_0 is supposed to equally cover the stretched surface. The induced magnetic and electric fields are disregarded since the magnetic Reynolds number is so low.

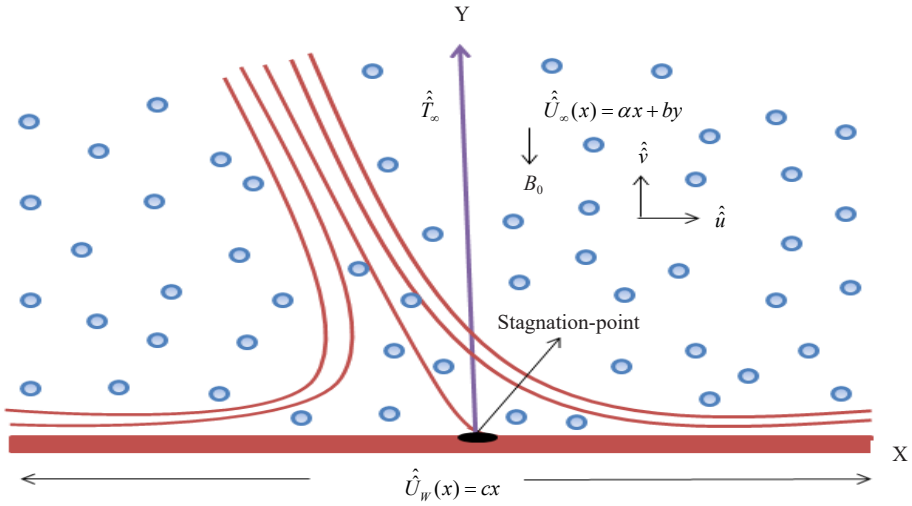

Figure 1. Physical model

The governing equations are given below [10], [11], [12], [16], [22], [25]

$$\frac{\partial \hat{u}}{\partial x} + \frac{\partial \hat{v}}{\partial y} = 0, \tag{1}$$

$$\hat{u}\frac{\partial \hat{u}}{\partial x} + \hat{v}\frac{\partial \hat{u}}{\partial y} = \hat{U}_\infty \frac{\partial \hat{U}_\infty}{\partial x} + \nu_f \frac{\partial^2 \hat{u}}{\partial y^2} + g\beta(\hat{T} - \hat{T}_\infty) + g\beta^*(\hat{C} - \hat{C}_\infty) - \left(\frac{\sigma B_0^{\,2}}{\rho_f} + \frac{\nu_f}{K}\right)\left(\hat{u} - \hat{U}_\infty\right), \tag{2}$$

$$\hat{u}\frac{\partial \hat{T}}{\partial x} + \hat{v}\frac{\partial \hat{T}}{\partial y} = \alpha_f \frac{\partial^2 \hat{T}}{\partial y^2} + \tau\left\{D_B\left(\frac{\partial \hat{C}}{\partial y}\frac{\partial \hat{T}}{\partial y}\right) + \frac{D_T}{T_\infty}\left(\frac{\partial \hat{T}}{\partial y}\right)^2\right\}, \tag{3}$$

$$\hat{u}\frac{\partial \hat{C}}{\partial x} + \hat{v}\frac{\partial \hat{C}}{\partial y} = D_B \frac{\partial^2 \hat{C}}{\partial y^2} + \frac{D_T}{T_\infty}\frac{\partial^2 \hat{T}}{\partial y^2}. \tag{4}$$

The boundary conditions are as follows [10], [16], [20], [22], [31], [33]

$$\hat{u} = \hat{U}_W = cx,\ \hat{v} = 0,\ -k\frac{\partial \hat{T}}{\partial y} = h_f\left(\hat{T}_f - \hat{T}\right),\ \hat{C} = \hat{C}_W \text{ at } y = 0, \tag{5}$$

$$\hat{u} = \hat{U}_\infty = ax + by,\ \hat{T} \to \hat{T}_\infty,\ \hat{C} \to \hat{C}_\infty \text{ as } y \to \infty. \tag{6}$$

Non-dimensional similarity variables are as follows:

$$\eta = y\sqrt{\frac{c}{\nu_f}},\ X = x\sqrt{\frac{c}{\nu_f}},\ u = \sqrt{c\nu_f}\left[Xf' + g'\right],\ v = -\sqrt{c\nu_f}\,f(\eta),$$

$$\psi = v_f\left[Xf(\eta)+g(\eta)\right],\ \theta(\eta)=\frac{\hat{\hat{T}}-\hat{\hat{T}}_\infty}{\hat{\hat{T}}_f-\hat{\hat{T}}_\infty},\ \phi(\eta)=\frac{\hat{\hat{C}}-\hat{\hat{C}}_\infty}{\hat{\hat{C}}_W-\hat{\hat{C}}_\infty}. \tag{7}$$

$\psi = v_f\left[Xf(\eta)+g(\eta)\right],$ is

$$\hat{\hat{u}}=\sqrt{\frac{c}{v_f}}\frac{\partial\psi}{\partial\eta},\ \hat{\hat{v}}=-\sqrt{\frac{c}{v_f}}\frac{\partial\psi}{\partial X}. \tag{8}$$

The normal and tangential parts of flow are represented here by $f(\eta)$ and $g(\eta)$.
Equation (1) is satisfied using (8) and equations (2) to (4) are reduced into ordinary equations as given below:

$$f'''+ff''-\left(f'\right)^2+\left(M+K_p\right)\left(\lambda_1-f'\right)+\lambda_1{}^2+Grt\theta+Grc\phi=0, \tag{9}$$

$$g'''+fg''-f'g'+\left(M+K_p\right)\left(\lambda_2\eta-g'\right)+\lambda_2 S=0, \tag{10}$$

$$\theta''+\Pr\left\{f\theta'+Nb\phi'\theta'+Nt\left(\theta'\right)^2\right\}=0, \tag{11}$$

$$\phi''+\Pr Lef\phi'+\frac{Nt}{Nb}\theta''=0. \tag{12}$$

Boundary conditions (5) and (6) are transformed as follows:

$$f=0,\ f'=1,\ g'=0,\ \theta'=-Bi\left[1-\theta(\eta)\right],\ \phi=1 \text{ at } \eta=0, \tag{13}$$

$$f'=\lambda_1,\ g''=\lambda_2,\ \theta\to 0,\ \phi\to 0 \text{ as } \eta\to\infty. \tag{14}$$

From equation (14), it can be easily seen that $f(\eta)=\lambda_1\eta+S$ as $\eta\to\infty$.

$$\text{Let } g^1=\lambda_2 G(\eta). \tag{15}$$

Substituting equation (15) into equations (10), (13), and (14):

$$G''(\eta)+fG'(\eta)-f'G(\eta)+\left(M+K_p\right)\left(\eta-G(\eta)\right)+S=0, \tag{16}$$

$$f=0,\ f'=1,\ G=0,\ \theta'=-Bi\left[1-\theta(\eta)\right],\ \phi=1 \text{ at } \eta=0, \tag{17}$$

$$f'=\lambda_1,\ G'=1,\ G'=1,\ \phi\to 0 \text{ as } \eta\to\infty. \tag{18}$$

The parameters are defined as:

$$\lambda_1 = \frac{a}{c},\ \lambda_2 = \frac{b}{c},\ Nt = \frac{\tau D_T\left(\hat{\hat{T}}_f - \hat{\hat{T}}_\infty\right)}{v_f \hat{\hat{T}}_\infty},\ Nb = \frac{\tau D_B\left(\hat{\hat{C}}_W - \hat{\hat{C}}_\infty\right)}{v_f},\ \Pr = \frac{v_f}{\alpha_f},\ v_f = \frac{\mu_f}{\rho_f},\ Le = \frac{\alpha_f}{D_B},$$

$$M = \frac{\sigma B_0^{\ 2}}{\rho_f c},\ Bi = \frac{h_f}{k}\sqrt{\frac{v_f}{c}},\ \alpha_f = \frac{k}{\left(\rho c_p\right)_f},\ K_p = \frac{v_f}{cK},\ Grt = \frac{g\beta\left(\hat{\hat{T}}_f - \hat{\hat{T}}_\infty\right)}{c^2 x},\ Grc = \frac{g\beta^*\left(\hat{\hat{C}}_W - \hat{\hat{C}}_\infty\right)}{c^2 x}. \tag{19}$$

Where C_f, Nu_x, and Sh_x are given below:

$$C_f = \frac{\tau_W}{\rho_f U_W^{\ 2}},\ Nu_x = \frac{xq_W}{k(\hat{\hat{T}}_f - \hat{\hat{T}}_\infty)}, \text{ and } Sh_x = \frac{xq_m}{k(\hat{\hat{C}}_W - \hat{\hat{C}}_\infty)}. \tag{20}$$

$$\tau_W = \mu_f\left(\frac{\partial \hat{\hat{u}}}{\partial y}\right)_{y=0},\ q_W = -k\left(\frac{\partial \hat{\hat{T}}}{\partial y}\right)_{y=0}, \text{ and } q_m = -D_B\left(\frac{\partial \hat{\hat{C}}}{\partial y}\right)_{y=0}. \tag{21}$$

Using equation (23) in equation (22), we obtain

$$C_f = \left(Xf''(0) + g''(0)\right),\ Nu_x = -\theta'(0), \text{ and } Sh_x = -\phi'(0). \tag{22}$$

3. Method of solution

The differential transform of the derivative of j[th] function $u(\eta)$ is,

$$U[j] = \frac{1}{j!}\left[\frac{d^j u(\eta)}{d\eta^j}\right]_{\eta=\eta_0}, \tag{23}$$

Here, $u(\eta)$ gives the original and $U(j)$ is transformed functions. Inverse differential transform is,

$$u(\eta) = \sum_{j=0}^{\infty} F(j)(\eta - \eta_0)^j, \tag{24}$$

In real-world problems, we represent $u(\eta)$ in finite series and given below,

$$u(\eta) = \sum_{j=0}^{m} U(k)(\eta - \eta_0)^j. \tag{25}$$

Here, m is calculated by the convergence in this study.

The reduced governing equations (9), (11), (12), and (16) with the boundary conditions (17) and (18) are resolved by using the DTM method and we get the following equations (26) to (29).

$$(i+1)(i+2)(i+3)F[k+3]+\sum_{r=0}^{i}(i+1)F[i-r](i+2)F[i+2]$$

$$-\sum_{r=0}^{i}(i+1)(i-r+1)F[i-r+1]F[i+1]-(i+1)(M+K_p)F[i+1]+\left[(M+K_p)\lambda_1+\lambda_1^{\,2}\right]\delta(i)+GrtT[i]+GrcP[i]=0, \tag{26}$$

$$(i+1)(i+2)T[i+2]+\Pr\left\{\sum_{r=0}^{i}(r+1)F[i-r]T[r+1]+Nb\sum_{r=0}^{i}(r+1)T[i-r+1](i-r+1)P[r+1]\right\}+$$

$$\Pr\left\{Nt\sum_{r=0}^{i}(i+1)T[i-r+1](i-r+1)T[i+1]\right\}=0, \tag{27}$$

$$(i+1)(i+2)P[i+2]+\Pr Le\left\{\sum_{r=0}^{i}(r+1)F[i-r]P[r+1]\right\}+(i+1)\frac{Nt}{Nb}(i+2)T[i+2]=0, \tag{28}$$

$$(i+1)(i+2)H[i+2]-\sum_{r=0}^{i}(r+1)H[i-r]F[r+1]+\sum_{r=0}^{i}(r+1)F[i-r]H[r+1]-(M+K_p)H[i]+(M+K_p)\delta(i-1)+S\delta(i)=0. \tag{29}$$

Transformed boundary conditions are:

$$F[0]=0,\ F[1]=1,\ F[2]=\frac{b}{2},\ H[0]=0,\ H[1]=e,\ T[0]=\frac{Bi-c}{Bi},$$

$$T[1]=c,\ P[0]=1,\ P[1]=d. \tag{30}$$

Differential transform of $f(\eta)$, $\theta(\eta)$, $\phi(\eta)$, $G(\eta)$ are $F(i)$, $T(i)$, $P(i)$, $H(i)$ and with the help of boundary conditions (17) and (18), we can find constants b, c, d, and e. By using transformed boundary conditions (30) and equations (26) to (29), we obtain the closed form of solution.

By using equation (30), we get the following iterations:

$$F[3]=\frac{1}{6}\left[1+(M+K_p)-\left\{\lambda_1(M+K_p)+\lambda_1^{\,2}\right\}-Grc+Grt\left(\frac{Bi-c}{Bi}\right)\right],...$$

$$T[2]=-\frac{1}{2}\left[\Pr Nbcd+\Pr Ntc^2\right],...$$

$$P[2]=\frac{1}{2}\frac{Nt}{Nb}\left[\Pr Nbcd+\Pr Ntc^2\right],...$$

$$G[2]=-\frac{S}{2},\ G[3]=-\frac{1}{6}\left[\left(M+K_p\right)-\left(M+K_p\right)e\right],...$$

Putting these iterations in equation (25), we obtain the closed form of solutions.

4. Result and discussion

The results are shown in Figures 2 to 20 and explored in detail to demonstrate the characteristics of the problem. Sh_x, Nu_x, and C_f, are all tabulated. The accuracy of the acquired results are checked and an excellent agreement is found, which are mentioned in Table 1 and Table 2.

Table 1. Coefficient of $f'(0)$ with $M = 0$, $K_p = 0$, $\beta = 0$

λ_1	S Present	$f''(0)$ Present	$G'(0)$ Present	S Makindeet al. [10]	$f''(0)$ Makindeet al. [10]	$G'(0)$ Makindeet al. [10]
0.1	-0.791705	-0.969386	0.26332	-0.791705	-0.969386	0.26332
0.2	-	-0.919209	-	-	-	-
0.3	-0.519499	-0.849420	0.60631	-0.519499	- 0.849420	0.60631
0.8	-	-	-	-0.114527	-0.299388	0.93472
2	0.410407	2.017502	1.16521	0.410407	2.017502	1.16521
3	0.693053	4.729282	-	0.693053	4.729282	1.23465

Table 2. Comparison with Makinde et al. [10] with $\lambda_1 = \beta = Nr = M = K_p = 0$, Pr = 10, $Le = 10$, $Bi = 0.1$

Nt	$-\theta'(0)$ $Nb = 0.1$ Present	$-\phi'(0)$ $Nb = 0.1$ Present	$-\theta'(0)$ $Nb = 0.5$ Present	$-\phi'(0)$ $Nb = 0.5$ Present	$-\theta'(0)$ $Nb = 0.1$ Makinde et al. [10]	$-\phi'(0)$ $Nb = 0.1$ Makinde et al. [10]	$-\theta'(0)$ $Nb = 0.5$ Makinde et al. [10]	$-\phi'(0)$ $Nb = 0.5$ Makinde et al. [10]
0.1	0.092135	2.277412	0.038331	2.356031	0.0921	2.27741	0.03833	2.35603
0.2	0.092551	2.222812	0.026901	2.457621	0.09255	2.22281	0.02690	2.45762
0.3	0.092121	2.178343	0.018001	2.543524	0.09212	2.17834	0.01800	2.54352

4.1 *Velocity profile*

The impact of magnetic parameter M on the axial and oblique velocity gradient profiles (i.e., $f'(\eta)$ and $G'(\eta)$) in the boundary layer is seen in Figures 2 and 7. The Lorentz force is a resistive-type force that occurs when a transverse magnetic field is applied to an electrically conducting fluid and has the propensity to slow down the fluid in the boundary layer. As a result, $f'(\eta)$ and $G'(\eta)$ both drop. Figures 3 and 8 show that the axial velocity, as well as oblique velocity gradient profiles, diminishes as the values of the porosity parameter K_p increases. Because increasing K_p amplifies the porous layer and thereby reduces the thickness of the momentum boundary layer. In Figures 4 and 5, as the values of the thermal Grashof number Grt and the solutal Grashof number Grc rise, $f'(\eta)$ and $G'(\eta)$ also rise. The ratio of the buoyant force to the viscous force is known as Grt. It is noted that the flow is accelerated due to the increase in the buoyant force in accordance with the rising thermal Grt for fluids. The buoyant force to viscous hydrodynamic force ratio is known as Grc. Thus, as hydrodynamic force increases and buoyancy force remains constant, the thickness of the momentum boundary layer decreases. The result of the velocity ratio parameter λ_1 on $f'(\eta)$ and $G'(\eta)$ is depicted in Figures 6 and 9. When $U_e(x)$ exceeds $U_w(x)$, the flow velocity rises, and the thickness of the boundary layer reduces as λ_1 rises. Furthermore, when $U_e(x) < U_w(x)$, the flow field velocity reduces. The flow exhibits an inverted boundary layer structure when $\lambda_1 < 1$.

4.2 *Temperature and nanoparticles volume fraction Profiles*

The effect of M on $\theta(\eta)$ and $\phi(\eta)$ in the boundary layer is demonstrated in Figures 10 and 19. The Lorentz force is a resistive-type force that is produced when a transverse magnetic field is applied to an electrically conducting fluid. This force tends to raise its temperature in the boundary layer and create a higher concentration of nanoparticles in the fluid. In addition, when the magnetic field intensity increases, the impacts on flow and heat fields become more prominent. As shown in Figure 11, the temperature profile rises when K_p rises.

Due to the expansion of the fluid's pores, K_p develops a resistance force that opposes the flow field and rises and thickens the thermal boundary layer. The effect of the Biot number Bi on the thermal boundary layer is depicted in Figure 12. Higher surface temperatures are caused by stronger convection, which increases the thermal effect to penetrate deeper into the static fluid, as predicted. The effect of the Brownian motion parameter Nb and thermophoresis parameter Nt on $\theta(\eta)$ is given in Figures 13 and 14. The random motion of nanoparticles increases, as and increases. More heat is generated by the nanoparticles' random motion. As a result, $\theta(\eta)$ rises. According to Figure 15, as λ_1 is increased, the dimensionless $\theta(\eta)$ decreases, reducing the thickness of the thermal boundary layer and subsequently the thermal resistance. Whereas, Figure 16 shows that as the Prandtl number Pr increases, $\theta(\eta)$ reduces. Larger viscous diffusivity and weaker thermal diffusivity can be seen in fluids having higher Pr. Because of this variation in fluids, thermal boundary layer thickness reduces. Hence, $\theta(\eta)$ reduces. Figure 17 shows that as the Lewis number Le rises, nanoparticle volume fraction profile (i.e., $\phi(\eta)$) degrades. Le and Brownian diffusion coefficient are of opposite behavior. As Le raises Brownian diffusion coefficient reduces. $\phi(\eta)$ grows as Nt increases, as shown in Figure 18. In reality, as Nt rises, the variation in temperature between the wall and the free surface also rises, which improves the concentration of the nanofluid.

4.3 *Streamlines*

Figures 20 to 22 show streamlined patterns for oblique flow. The streamlines are inclined left for positive values of λ_2 as shown in Figure 19 and right for negative values of the velocity ratio parameter λ_2 in Figure 22, as expected. When $\lambda_2 = 0$, the streamlines are found to be normal to the surface in Figure 21. This is because rising λ_2 enhances shearing motion, which causes the flow to become increasingly obliquity towards the stretched surface.

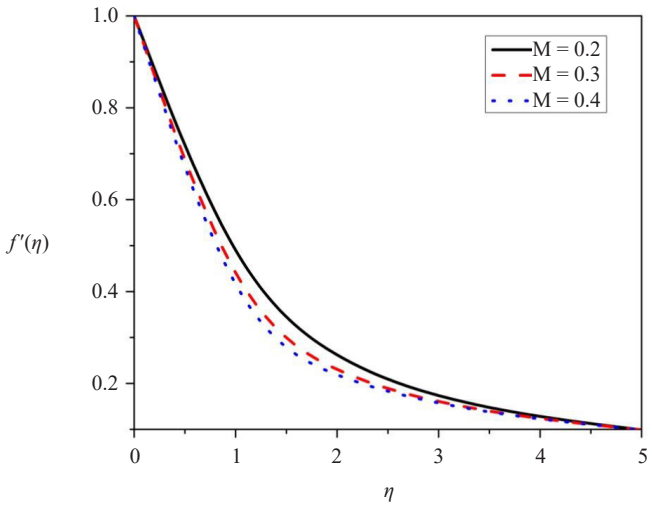

$\lambda_1 = 0.1,\ Bi = 0.1,\ Nb = 0.5,\ Grt = 0.2,\ Nt = 0.5,\ K_p = 0.5,\ Grc = 0.2,\ Le = 5,\ \mathrm{Pr} = 2$

Figure 2. Variation of $f'(\eta)$ on M

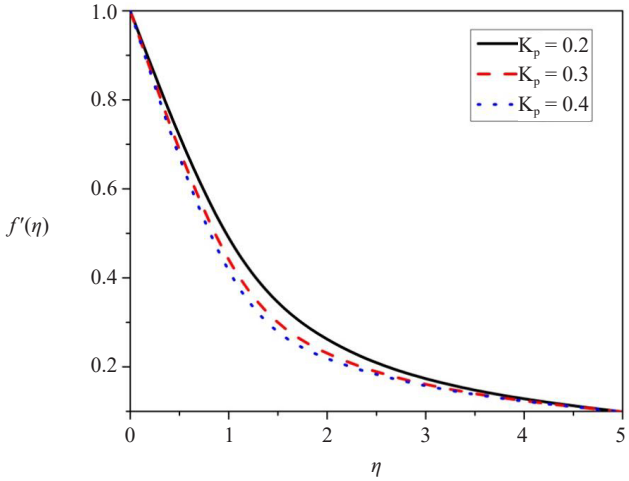

$\lambda_1 = 0.1$, $Bi = 0.1$, $Nb = 0.5$, $Grt = 0.2$, $M = 0.3$, $Nt = 0.5$, $Grc = 0.2$, $Le = 5$, Pr = 2

Figure 3. Variation of $f'(\eta)$ on K_p

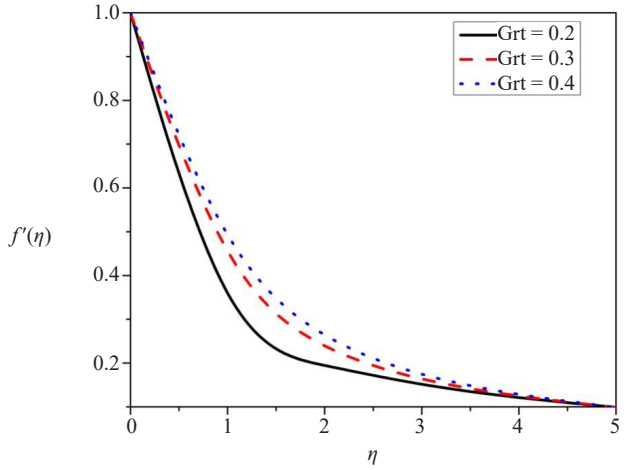

$\lambda_1 = 0.1$, $Bi = 0.1$, $Nb = 0.5$, $K_p = 0.3$, $M = 0.3$, $Nt = 0.5$, $Grc = 0.2$, $Le = 5$, Pr = 2

Figure 4. Variation of $f'(\eta)$ on Grt

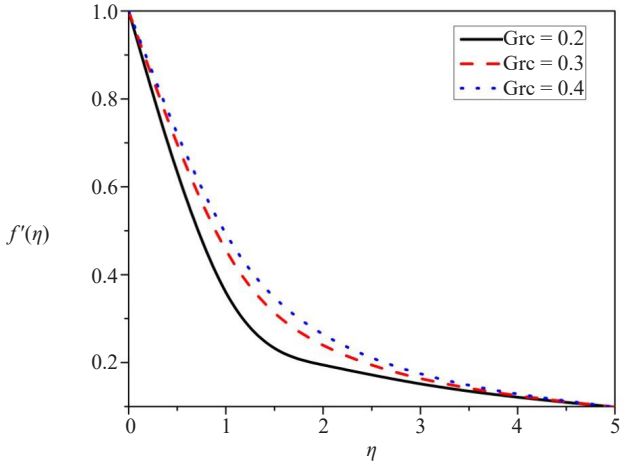

$\lambda_1 = 0.1$, $Bi = 0.1$, $Nb = 0.5$, $K_p = 0.3$, $M = 0.3$, $Nt = 0.5$, $Grt = 0.2$, $Le = 5$, Pr = 2

Figure 5. Variation of $f'(\eta)$ on Grc

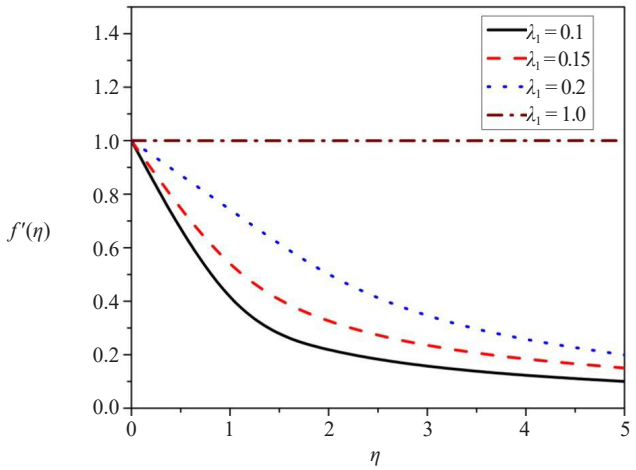

Grc = 0.2, *Bi* = 0.1, *Nb* = 0.5, K_p = 0.3, *M* = 0.3, *Nt* = 0.5, *Grt* = 0.2, *Le* = 5, Pr = 2

Figure 6. Variation of $f'(\eta)$ on λ_1

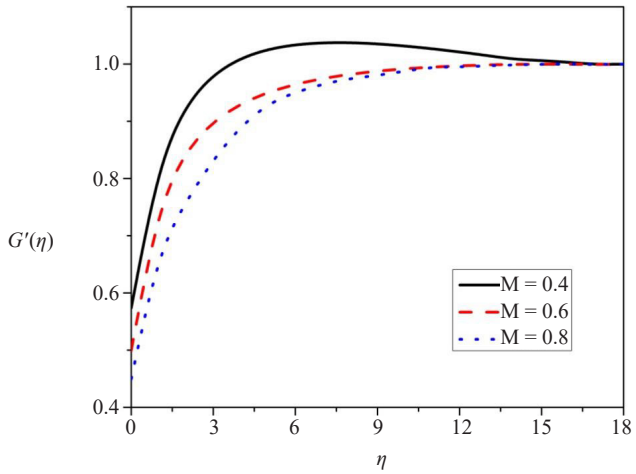

Grc = 0.3, *Bi* = 0.2, *Nb* = 0.3, K_p = 0.7, *Nt* = 0.3, *Grt* = 0.3, *Le* = 100, Pr = 2, λ_1 = 0.1, *S* = -0.45

Figure 7. Variation of $G'(\eta)$ on *M*

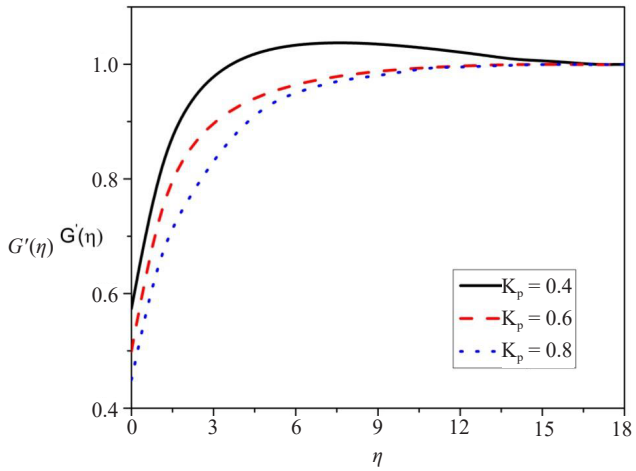

Grc = 0.3, *Bi* = 0.2, *Nb* = 0.3, *M* = 0.7, *Nt* = 0.3, *Grt* = 0.3, *Le* = 100, Pr = 2, λ_1 = 0.1, *S* = -0.45

Figure 8. Variation of $G'(\eta)$ on K_p

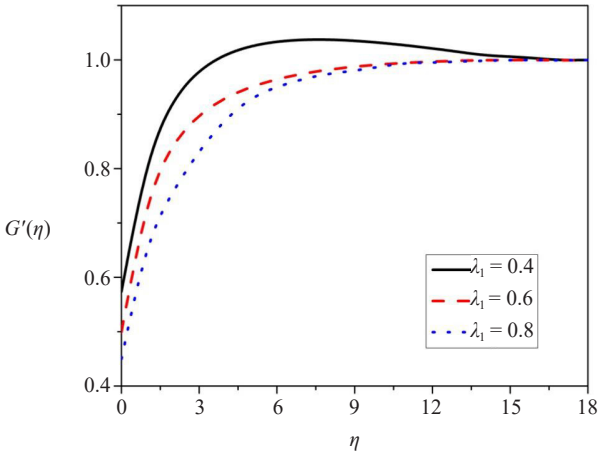

$Grc = 0.3$, $Bi = 0.2$, $Nb = 0.3$, $M = 0.7$, $Nt = 0.3$, $Grt = 0.3$, $Le = 100$, Pr = 2, $K_p = 0.7$, $S = -0.45$

Figure 9. Variation of $G'(\eta)$ on λ_1

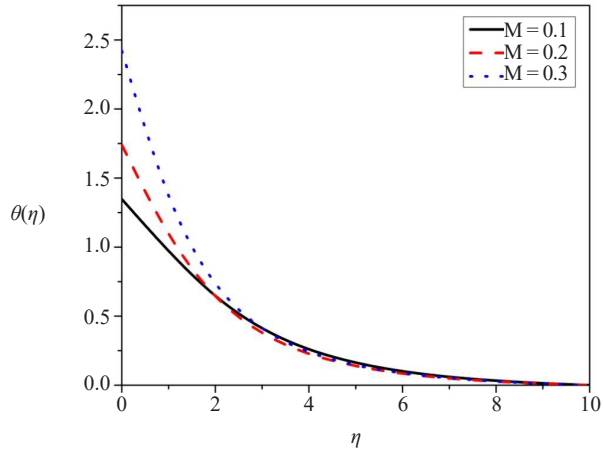

$Grc = 0.1$, $Nt = 0.1$, $Grt = 0.1$, $Le = 100$, Pr = 1, $K_p = 0.3$, $\lambda_1 = 0.1$, $Nb = 0.1$

Figure 10. Variation of $\theta(\eta)$ on M

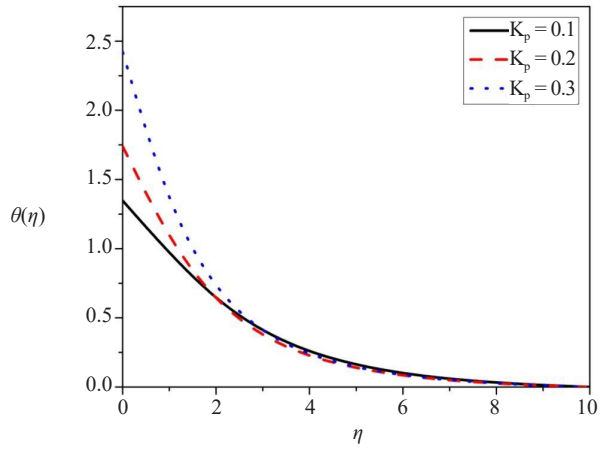

$Grc = 0.1$, $Nt = 0.1$, $Grt = 0.1$, $Le = 100$, Pr = 1, $\lambda_1 = 0.1$, $Nb = 0.1$

Figure 11. Variation of $\theta(\eta)$ on K_p

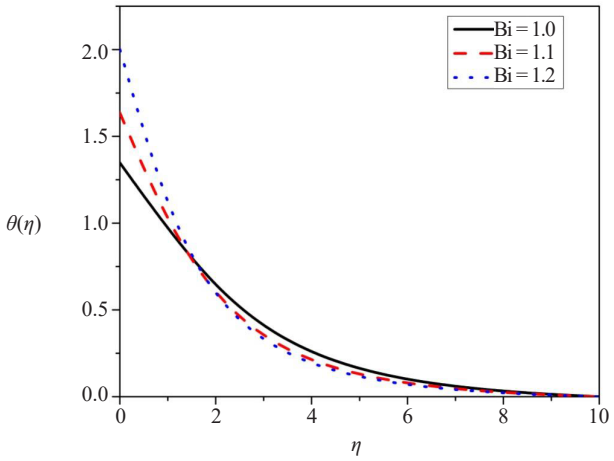

$Grc = 0.1$, $Nb = 0.1$, $M = 0.3$, $Nt = 0.1$, $Grt = 0.1$, $Le = 100$, Pr = 1, $K_p = 0.3$, $\lambda_1 = 0.1$

Figure 12. Variation of $\theta(\eta)$ on Bi

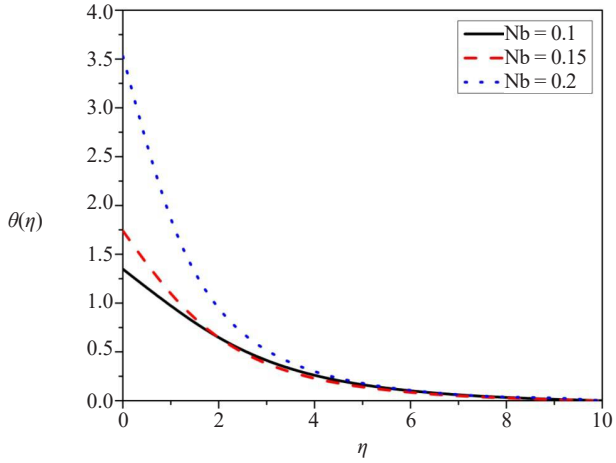

$Grc = 0.1$, $Bi = 1$, $M = 0.3$, $Nt = 0.1$, $Grt = 0.1$, $Le = 100$, Pr = 1, $K_p = 0.3$, $\lambda_1 = 0.1$

Figure 13. Variation of $\theta(\eta)$ on Nb

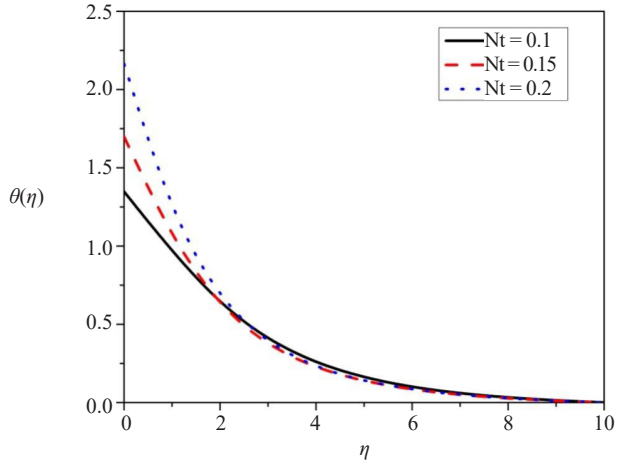

$Grc = 0.1$, $Bi = 1$, $M = 0.3$, $Nb = 0.1$, $Grt = 0.1$, $Le = 100$, Pr = 1, $K_p = 0.3$, $\lambda_1 = 0.1$

Figure 14. Variation of $\theta(\eta)$ on Nt

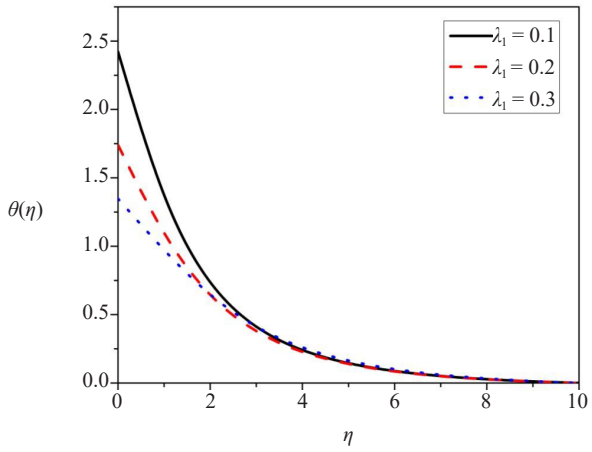

$Grc = 0.1$, $Bi = 1$, $M = 0.3$, $Nb = 0.1$, $Grt = 0.1$, $Le = 100$, $Nt = 0.1$, $K_p = 0.3$, $\mathrm{Pr} = 1$

Figure 15. Variation of $\theta(\eta)$ on λ_1

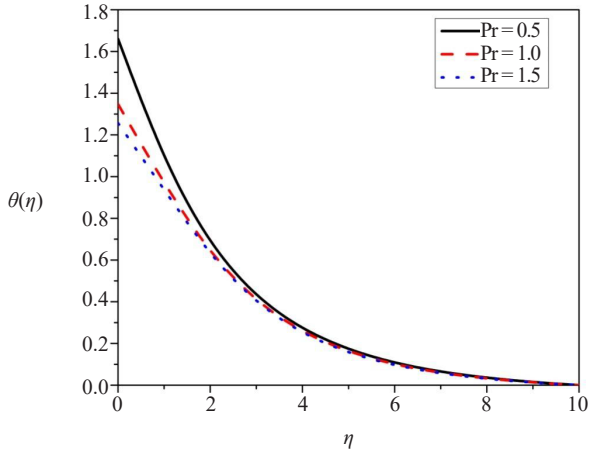

$Grc = 0.1$, $Bi = 1$, $M = 0.3$, $Nb = 0.1$, $Grt = 0.1$, $Le = 100$, $Nt = 0.1$, $K_p = 0.3$, $\lambda_1 = 0.1$

Figure 16. Variation of $\theta(\eta)$ on Pr

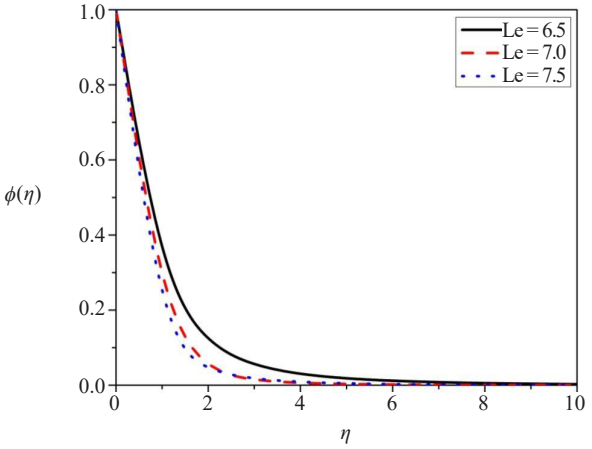

$Grc = 0.1$, $Bi = 0.1$, $M = 0.3$, $Nb = 0.1$, $Grt = 0.1$, $Nt = 0.1$, $K_p = 0.3$, $\mathrm{Pr} = 1$

Figure 17. Variation of $\phi(\eta)$ on Le

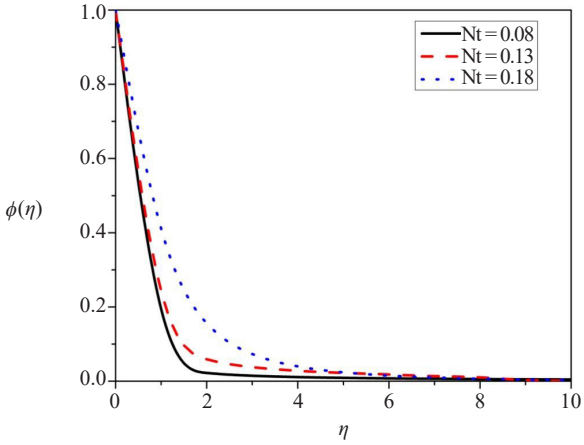

$Grc = 0.1$, $Bi = 0.1$, $M = 0.3$, $Nb = 0.1$, $Grt = 0.1$, $\lambda_1 = 0.1$, $K_p = 0.3$, Pr = 1

Figure 18. Variation of $\phi(\eta)$ on Nt

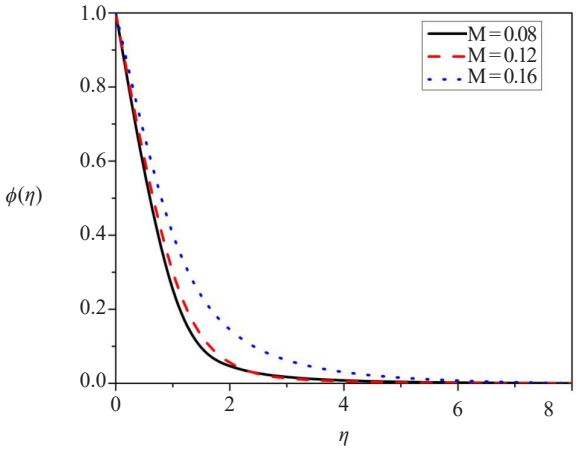

$Grc = 0.1$, $Bi = 0.1$, $Nt = 0.1$, $Nb = 0.1$, $Grt = 0.1$, $\lambda_1 = 0.1$, $K_p = 0.3$, Pr = 1

Figure 19. Variation of $\phi(\eta)$ on M

5. Conclusions

MHD Non-aligned stagnation-point flow of nanofluids over a stretching surface in a porous medium with a convective boundary condition has been studied by using DTM. The following is an overview of our findings:

• The axial velocity and oblique velocity gradient profiles exhibit similar behavior with M, but $\theta(\eta)$ and $\phi(\eta)$ exhibit the opposite tendency.

• As K_p values rise, the temperature profile rises, while the axial velocity and oblique velocity gradient profiles exhibit the opposite trend.

• The oblique velocity gradient and temperature profiles demonstrate similar patterns as λ_1 values rise.

• As Bi increases the temperature profile increases.

• The volume fraction profile of nanoparticles and temperature both increase as Nt increases.

• Streamline patterns for the oblique flow for varying λ_2 can be seen. This is because an increase in λ_2 increases the shearing action, which in turn causes the flow toward the stretched surface to be more, inclined.

• In Tables 1 and 2, the current findings are matched and validated against the information found in the literature. There is considerable agreement between our findings.

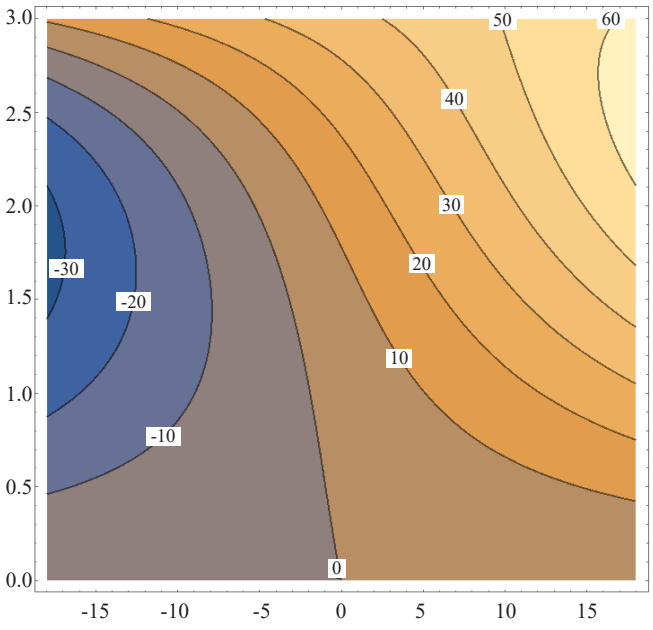

$Grc = 0.1$, $Bi = 0.1$, $Grt = 0.1$, $K_p = 0.5$, $\Pr = 6$, $M = 0.5$, $\lambda_1 = 0.1$, $\lambda_2 = 2.5$

Figure 20. Streamline patterns for the oblique flow for the above condition

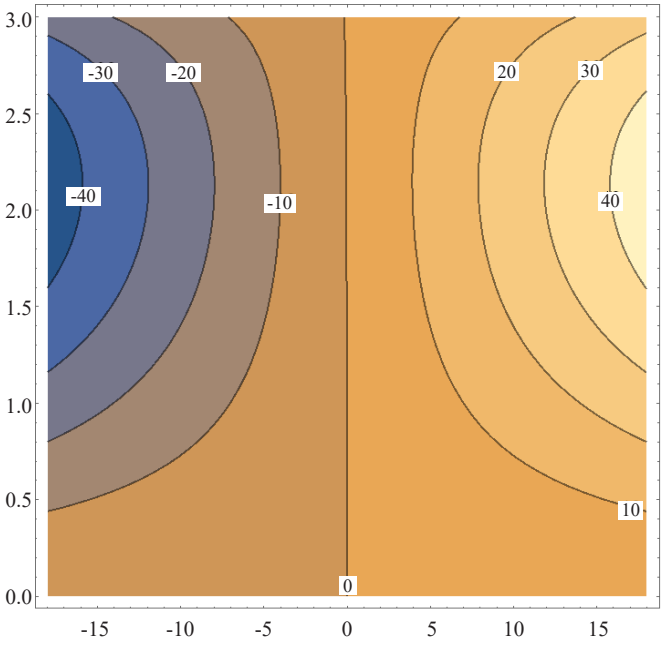

$Grc = 0.1$, $Bi = 0.1$, $Grt = 0.1$, $K_p = 0.5$, $\Pr = 6$, $M = 0.5$, $\lambda_1 = 0.1$, $\lambda_2 = 0$

Figure 21. Streamline patterns for the oblique flow for the above condition

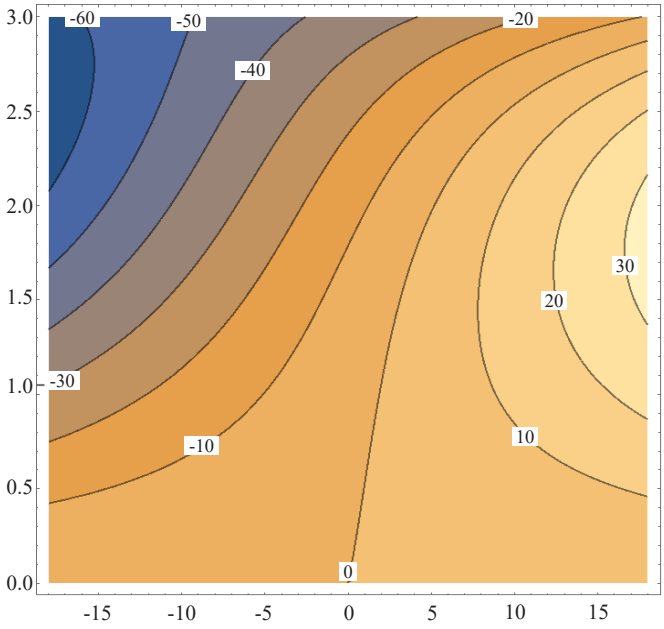

$Grc = 0.1$, $Bi = 0.1$, $Grt = 0.1$, $K_p = 0.5$, $\mathrm{Pr} = 6$, $M = 0.5$, $\lambda_1 = 0.1$, $\lambda_2 = -2.5$

Figure 22. Streamline patterns for the oblique flow for the above condition

Conflicts of interest

The authors declare that there are no relevant financial or non-financial interests.

References

[1] L. J. Crane, "Flow past a stretching plate," *Journal of Applied Mathematics and Physics*, vol. 21, pp. 645-647, 1970.

[2] G. I. Burde, "Non-steady Stagnation-Point flows over permeable surfaces: Explicit Solutions of the Navier-Stokes Equations," *Journal of Fluids Engineering*, vol. 117, no. 1, pp. 189-191, 1995.

[3] J. T. Stuart, "The viscous flow near a stagnation point when external flow has uniform vorticity," *Journal of the Aerospace Sciences*, vol. 26, pp. 124-125, 1959.

[4] K. Tamada, "Two-dimensional stagnation-point flow impinging obliquely on a plane wall," *Journal of the Physical Society of Japan*, vol. 46, no. 1, pp. 310-311, 1979.

[5] J. M. Dorrepaal, "An exact solution of the Navier Stokes equation which describes Non-orthogonal stagnation-point flow in two-dimensions," *Journal of Fluid Mechanics*, vol. 163, pp. 141-147, 1986.

[6] M. Reza and A. S. Gupta, "Steady two-dimensional oblique stagnation-point flow towards a stretching surface," *Fluid Dynamics Research*, vol. 37, no. 5, pp. 334-340, 2005.

[7] T. C. Chiam,"Stagnation-point flow towards a stretching plate," *Journal of the Physical Society of Japan*, vol. 63, no. 6, pp. 2443-2444, 1994.

[8] T. R. Mahapatra, S. K. Nandy, and A. S. Gupta, "Oblique stagnation-point flow and heat transfer towards a shrinking sheet with thermal radiation," *Meccanica*, vol. 47, pp. 1325-1335, 2012.

[9] S. Nadeem, R. Mehmood, and N. S. Akbar, "Non-orthogonal stagnation point flow of a nano non-Newtonian fluid towards a stretching surface with heat transfer," *International Journal of Heat and Mass Transfer*, vol. 57, no. 2, pp. 679-689, 2013.

[10] W. A. Khan, O. D. Makinde, and Z. H. Khan, "Non-aligned MHD stagnation point flow of variable viscosity nanofluids past a stretching sheet with radiative heat," *International Journal of Heat and Mass Transfer*, vol. 96, pp. 525-534, 2016.

[11] M. Jayachandra Babu and N. Sandeep, "Effect of nonlinear thermal radiation on non-aligned bio-convective

stagnation point flow of a magnetic-nanofluid over a stretching sheet," *Alexandria Engineering Journal*, vol. 55, no. 3, pp. 1931-1939, 2016.
[12] N. Vijaya, G. Venkata Ramana Reddy, and Y. Hara Krishna, "Non-aligned stagnation point flow of a casson fluid past a stretching sheet in a doubly stratified medium," *Fluid Dynamics & Materials Processing*, vol. 15, no. 3, pp. 233-251, 2019.
[13] M. R. Khan, K. Pan, A. Ullah Khan, and N. Ullah, "Comparative study on heat transfer in CNTs-water nanofluid over a curved surface," *International Communications in Heat and Mass Transfer*, vol. 116, pp. 104707, 2020.
[14] X. L. Li, A. Ullah Khan, M. R. Khan, S. Nadeem, and S. Ullah Khan, "Oblique stagnation point flow of nanofluids over stretching/shrinking sheet with cattaneo-christov heat flux model: Existence of dual solution," *Symmetry*, vol. 11, no. 9, pp. 1070, 2019.
[15] A. A. Raptis and H. S. Takhar, "Flow through a porous medium," *Mechanics Research Communications*, vol. 14, pp. 327-329, 1987.
[16] M. A. Seddeek, "Heat and mass transfer on a stretching sheet with a magnetic field in a visco-elastic fluid flow through a porous medium with heat source or sink," *Computational Materials Science*, vol. 38, no. 4, pp. 781-787, 2007.
[17] A. Rehman, S. Nadeem, and M. Y. Malik, "Stagnation flow of couple stress nanofluid over an exponentially stretching sheet through a porous medium," *Journal of Power Technologies*, vol. 93, no. 2, pp. 122-132, 2013.
[18] N. N. Reddy, V. S. Rao, and B. R. Reddy, "Chemical reaction impact on MHD natural convection flow through porous medium past an exponentially stretching sheet in presence of heat source/sink and viscous dissipation," *Case Studies in Thermal Engineering*, vol. 25, pp. 100879, 2021.
[19] A. M. Megahed and W. Abbas, "Non-Newtonian Cross fluid flow through a porous medium with regard to the effect of chemical reaction and thermal stratification phenomenon," *Case Studies in Thermal Engineering*, vol. 29, pp. 101715, 2022.
[20] N. S. Khan, S. Islam, T. Gul, I. Khan, W. Khan, and L. Ali, "Thin film flow of a second grade fluid in a porous medium past a stretching sheet with heat transfer," *Alexandria Engineering Journal*, vol. 57, no. 2, pp. 1019-1031, 2018.
[21] A. B. Jafar, S. Shafie, and I. Ullah, "MHD radiative nanofluid flow induced by a nonlinear stretching sheet in a porous medium," *Heliyon*, vol. 6, no. 6, pp. e04201, 2020.
[22] W. Ibrahim, B. Shankar, and M. M. Nandeppanavar, "MHD stagnation point flow and heat transfer due to nanofluid towards a stretching sheet," *International Journal of Heat and Mass Transfer*, vol. 56, no. 1-2, pp. 1-9, 2013.
[23] T. R. Mahapatra and A. S. Gupta, "Magnetohydrodynamics stagnation-point flow towards a stretching sheet," *Acta Mechanica*, vol. 152, pp. 191-196, 2001.
[24] A. Ishak, K. Jafar, R. Nazar, and I. Pop, "MHD stagnation point flow towards a stretching sheet," *Physica A: Statistical Mechanics and its Applications*, vol. 388, no. 17, pp. 3377-3383, 2009.
[25] P. Rajendar, L. Anand Babu, and T. Vijaya Laxmi, "MHD stagnation point flow and heat transfer due to nano fluid over exponential radiating stretching sheet," *Global Journal of Pure and Applied Mathematics*, vol. 13, no. 6, pp. 1593-1610, 2017.
[26] F. Mabood, W. A. Khan, and A. I. B. Md. Ismail, "MHD flow over exponential radiating stretching sheet using homotopy analysis method," *Journal of King Saud University - Engineering Sciences*, vol. 29, no. 1, pp. 68-74, 2017.
[27] E. Amos and U. A. Uka, "Hydromagnetic nanofluid flow over an exponentially stretching sheet in the presence of radiation and nonuniform heat generation/absorption," *IOSR Journal of Mathematics*, vol. 18, no. 1, pp. 31-43, 2022.
[28] B. Ali, A. Shafiq, I. Siddique, Q. Al-Mdallal, and F. Jarad, "Significance of suction/injection, gravity modulation, thermal radiation, and magnetohydrodynamic on dynamics of micropolar fluid subject to an inclined sheet via finite element approach," *Case Studies in Thermal Engineering*, vol. 28, pp. 101537, 2021.
[29] B. Ali, T. Thumma, D. Habib, N. Salamat, and S. Riaz, "Finite element analysis on transient MHD 3D rotating flow of Maxwell and tangent hyperbolic nanofluid past a bidirectional stretching sheet with Cattaneo Christov heat flux model," *Thermal Science and Engineering Progress*, vol. 28, pp. 101089, 2022.
[30] S. U. S. Choi and J. A. Eastman,"Enhancing thermal conductivity of fluid with nanoparticles," In Proc. ASME International Conference on Mechanical Engineering Congress & Exposition, 66, 1995, pp. 99-105.
[31] S. Nadeem, R. Mehmood, and N. S. Akbar, "Partial slip effect on non-aligned stagnation point nanofluid over a stretching convective surface," *Chinese Physics B*, vol. 24, no. 1, pp. 014702, 2015.
[32] W. A. Khan and I. M. Pop, "Boundary layer flow past a stretching surface in a porous medium saturated by a

nanofluid: Brinkman-forchheimer model," *PLoS One*, vol. 7, no.10, pp. e47031, 2012.
[33] S. Nadeem and R. UlHaq, "Effect of thermal radiation for megneto-hydrodynamic boundary layer flow of a nanofluid past a stretching sheet with convective boundary conditions," *Journal of Computational and Theoretical Nanoscience*, vol. 11, no. 1, pp. 32-40, 2014.
[34] S. Das, S. Chakraborty, R. N. Jana, and O. D. Makinde, "Entropy analysis of unsteady magneto-nanofluid flow past accelerating stretching sheet with convective boundary condition," *Applied Mathematics and Mechanics*, vol. 36, pp. 1593-1610, 2015.
[35] O. D. Makinde and A. Aziz, "Boundary layer flow of a nanofluid past a stretching sheet with a convective boundary condition," *International Journal of Thermal Sciences*, vol. 50, no. 7, pp. 1326-1332, 2011.
[36] J. K. Zhou, *Differential Transformation and Its Applications for Electrical Circuits*.Wuhan. Huazhong University of Science and Technology Press, 1986.
[37] C. K. Chen and S. H. Ho,"Solving partial differential equations by two-dimensional differential transform method," *Applied Mathematics and Computation*, vol. 106, no. 2-3, pp. 171-179, 1999.
[38] F. Ayaz, "Solutions of the system of differential equations by differential transform method," *Applied Mathematics and Computation*, vol. 147, no. 2, pp. 547-567, 2004.
[39] A. Arikoglu and I. Ozkol, "Solution of boundary value problems for integro-differential equations by using differential transform method," *Applied Mathematics and Computation*, vol. 168, no. 2, pp. 1145-1158, 2005.
[40] S. Sepasgozar, M. Faraji, and P. Valipour, "Application of differential transformation method (DTM) for heat and mass transfer in a porous channel," *Propulsion and Power Research*, vol. 6, no. 1, pp. 41-48, 2017.
[41] A. Mirzaaghaian and D. D. Ganji, "Application of differential transformation method in micropolar fluid flow and heat transfer through permeable walls," *Alexandria Engineering Journal*, vol. 55, no. 3, pp. 2183-2191, 2016.
[42] M. Hatami and D. Jing, "Differential transformation method for Newtonian and non-Newtonian nanofluids flow analysis: compared to numerical solution," *Alexandria Engineering Journal*, vol. 55, no. 2, pp. 731-739, 2016.